Research Square

Preprints are preliminary reports that have not undergone peer review.
They should not be considered conclusive, used to inform clinical practice,
or referenced by the media as validated information.

Year-Long Source Apportionment of $PM_{2.5}$ in Delhi: Insights from One of the World's Most Polluted Environments

Faisal Mohd

faisal.mohd@psi.ch

Paul Scherrer Institute

Ajit Kumar

Indian Institute of Technology Delhi

Manousos I. Manousakas

Institute of Nuclear & Radiological Sciences and Technology, Energy & Safety

Umer Ali

Indian Institute of Technology Delhi

Anna Tobler

Datalystica Ltd.

Laurence C. Windell

Paul Scherrer Institute

Jay G. Slowik

Paul Scherrer Institute

Sombir Pannu

Indian Institute of Technology Delhi

Vikram Singh

Indian Institute of Technology Delhi

Mayank Kumar

Indian Institute of Technology Delhi

André S. H. Prévôt

Paul Scherrer Institute

Article

Keywords:

Posted Date: November 11th, 2026

DOI: https://doi.org/10.21203/rs.3.rs-11501674/v1

License: This work is licensed under a Creative Commons Attribution 4.0 International License.
Read Full License

Additional Declarations: No competing interests reported.

Year-Long Source Apportionment of $PM_{2.5}$ in Delhi: Insights from One of the World's Most Polluted Environments

Mohd Faisal[1,2*], Ajit Kumar[3], Manousos I. Manousakas[4], Umer Ali[2], Anna Tobler[1], Laurence C. Windell[1], Jay G. Slowik[1], Sombir Pannu[2], Vikram Singh[2]*, Mayank Kumar[3], and André S. H. Prévôt*[1]

[1] PSI Center for Energy and Environmental Sciences, Paul Scherrer Institute, 5232 Villigen, Switzerland
[2] Department of Chemical Engineering, Indian Institute of Technology Delhi, New Delhi, India
[3] Department of Mechanical Engineering, Indian Institute of Technology Delhi, New Delhi, India
[4] Institute of Nuclear & Radiological Sciences and Technology, Energy & Safety, N.C.S.R. "Demokritos", 15310 Agia Paraskevi, Greece

*Corresponding Authors:
E-mail addresses: faisal.mohd@psi.ch (Mohd Faisal), andre.prevot@psi.ch (André S. H. Prévôt), vs225@chemical.iitd.ac.in (Vikram Singh).

Abstract

Delhi experiences some of the world's highest urban fine particulate matter ($PM_{2.5}$) concentrations, with most previous studies focusing on short-term source apportionment. Here, we present a long-term, multi-season characterization of $PM_{2.5}$ composition taking measurement from ACSM, Xact and Aethalometer (AXA). High time-resolved measurements of non-refractory $PM_{2.5}$ (NR-$PM_{2.5}$), elements, and black carbon (BC) were integrated to construct a composition-resolved metric (C-$PM_{2.5}$ = NR-$PM_{2.5}$ + elements + BC). Seasonal mean C-$PM_{2.5}$ concentrations were 210.2, 103.9, 60.6, 158.9, and 156.2 μg m^{-3} during early winter, spring, summer, autumn, and late winter, respectively. Organic aerosol (OA) dominated across all seasons (40–65%), with maxima in autumn (65.3%). Secondary inorganic aerosols (SO_4^{2-}, NO_3^-, NH_4^+, Cl^-) peaked in winter, while chloride also exhibited episodic summer events. Elemental contributions were elevated in summer (11%), with dust prevailing in summer. BC contributed 6–14% consistently. Positive matrix factorization (PMF) of OA was performed using rolling window approach using 21 days moving window in Sofi Pro , which resolved OA into hydrocarbon-like OA(HOA), fresh and aged biomass burning OA(BBOA-Fresh and BBOA-Aged), and oxygenated OA Less-oxidized oxygenated organic aerosol (LO-OOA) and more-oxidized oxygenated organic aerosol (MO-OOA). Elemental-PMF identified eight sources, including power plants, dust, biomass burning, traffic, secondary chloride, waste incineration, Pb-rich, and industrial emissions, with fireworks appearing episodically during Diwali in autumn. Source contributions exhibited strong seasonal variability, with dust dominating in summer and power plant (Sulphur rich) emissions in winter. This study provides the first integrated seasonal perspective on long-term $PM_{2.5}$ sources and transformation processes in Delhi, offering critical insights for air quality management.

1.Introduction

Delhi ranks among the most polluted capital cities globally in terms of its environmental performance index [1]. Delhi's PM_{10} level is alarmingly high [2]. Recent observations in Delhi have revealed it to be the world's most polluted megacity, with annual mean $PM_{2.5}$ levels of 140 μg/m^3 [3]. Researchers have reported public health issues from higher atmospheric pollution [4,5]. Therefore, identifying and apportioning aerosol sources is crucial for developing effective strategies to assess air quality control, understand climate change impacts, evaluate the health effects of particulate matter (PM), and implement PM mitigation measures.

Most of the studies in Delhi have primarily focused on analysing the chemical composition and identifying sources using a filter-based method with limited time resolution. However, this approach fails to capture

the dynamic changes in sources and may be prone to measurement artifacts [6–9]. Several source apportionment studies using on-line instrumentation over rather short periods have been conducted in Delhi recently, focusing on organic and elemental data [10–17]. These studies have provided valuable insights into Delhi's composition and sources of particulate air pollution. According to these on-line source apportionment studies, a significant proportion of Delhi's ambient air particulate matter is attributed to secondary organic aerosols (SOA) (40-60%), traffic emissions (20-30%), biomass burning (BB) (25-35%) [12,18,19]. Here, we collected high-time-resolution data of different components of $PM_{2.5}$ (C-$PM_{2.5}$), which is the sum of non-refractory $PM_{2.5}$ (NR-$PM_{2.5}$), elements, and BC, in Delhi using three real-time instruments (Q-ACSM, Xact, and Aethalometer (AE33)) over multiple seasons in contrast to most campaign studies over a few weeks. The present study will shed light on the atmospheric processsing and the particulate matter sources in the Indo-Gangetic Plain.

We performed a detailed long-term investigation of $PM_{2.5}$ composition and its sources, including different components of $PM_{2.5}$ (organics, elements, and black carbon) in different seasons.

2.Material and Methods

Delhi undergoes significant seasonal and diurnal fluctuations in temperature (T), relative humidity (RH), and wind speeds Fig. S1. We conducted sampling in five different seasons of 2022: (a) Early winter (W) (10^{th} January to 15^{th} February) and Late winter (1^{st} December to 31^{st} December) (characterized by mild temperature with 10-20 C mean diurnal variation, RH levels varying from 45 % to 90 %, and low wind speeds variation (~2–3 m/s). Summers (S) (1^{st} April to 10^{th} June) are scorching (T~24–42 ∘C) and dry (RH ~25%–60 %). Spring (Sp)(16^{th} February to 30^{th} March) and autumn (Au)(1^{st} October to 30^{th} November) have a transition season from winter to summer and vice versa.

We installed a set of high-resolution online instruments at the Indian Institute of Technology Delhi (IIT Delhi) campus, located in South Delhi, India (28.5505° N, 77.1830° E). The instruments were placed in a temperature (25 C)-regulated laboratory on the highest floor of a four-floor building and about 15 m above the ground.

We deployed a Quadruple-Aerosol Chemical Speciation Monitor (Q-ACSM) with a capture vaporizer to measure the non-refractory component of $PM_{2.5}$ (NR-$PM_{2.5}$) that includes OA, SO_4^{-2}, NO_3^-, NH_4^+, and Cl^-. To measure the elemental $PM_{2.5}$ ($PM_{2.5}$ el) composition, we deployed Xact 625i ambient metals monitor that measures a wide range of elements [20,21] . A multichannel Aethalometer (AE 33) was deployed to measure ambient BC [22] . The quality assurance or quality control (QA/QC) tests involved measuring the total $PM_{2.5}$[10] . More details about (QA/QC) are discussed in the supplementary section S1. The hourly measurements of meteorological parameters (temperature, RH, visibility, and wind speed) are measured at the nearest (3 Kms away) monitoring station operated by the Delhi pollution control Committee (DPCC),

R.K. Puram . Regional planetary boundary layer height (PBLH) data was obtained from the National Aeronautics and Space Administration (NASA) meteorological reanalysis dataset, MERRA2. The dataset is available at https://www.disc.gsfc.nasa.gov/. The global radiation data for Delhi was obtained from the European Centre for Medium-Range Weather Forecasts ECMWF-ERA5 reanalysis dataset. The fire count data is obtained by downloading the NRT VIIRS 375 m Active Fire product VNP14IMGT, which NASA FIRMS releases (https://earthdata.nasa.gov/data/near-real-time-data) .It was downloaded for 200 km radius of the sampling site. Organic aerosol and elemental source apportionment were performed using the rolling-window positive matrix factorization (PMF) approach implemented in SoFi with the ME-2 engine [11,23–26]. Black carbon source apportionment was conducted using the aethalometer model [27]. Details about the source apportionment method is discussed in S2 of supplementary section.

3 Results and Discussion

This section discusses the variation in the chemical composition and sources of $PM_{2.5}$ during the study period.

3.1 Variation of $PM_{2.5}$ mass and chemical composition on seasonal basis

Notable variations in the $PM_{2.5}$ mass levels were observed throughout different seasons and times of day, which can be attributed to the interplay between various pollutants, atmospheric interactions, and physical-chemical processes. Fig. 1 and Fig. S3 depicts the temporal variation of individual C-$PM_{2.5}$ species. The mean winter and autumn NR-$PM_{2.5}$ concentrations were about three times higher than in summer (Fig. 1). On most days, the daily mean $PM_{2.5}$ concentration went beyond the Indian National Ambient Air Quality Standards (NAAQS; 60 $\mu g/m^3$), and it surpassed the WHO 24 h mean air quality guidelines (5 $\mu g/m^3$) every day. Delhi's wintertime air pollution stands out due to the almost complete lack of clean air periods, unlike other very polluted megacities like Beijing, which experience intermittent fluctuations between clean and polluted conditions [28]. During the winter season, the daily mean $PM_{2.5}$ levels surpassed 100 $\mu g/m^3$ on 94% of the days, the Indian National Ambient Air Quality Standards (NAAQS) and the World Health Organization (WHO) recommendations on all days.

Seasonal variation in $PM_{2.5}$ mass concentration follows the variation in meteorological parameters like boundary layer height (BLH), wind speed, and RH. Fig. S1 shows the season-averaged diurnal variations of meteorological parameters. Lower wind speeds, high RH, and low BLH during the winter season result in the highest concentration of $PM_{2.5}$ throughout the year. However, during the summer season, the meteorological parameters favor the dispersion of pollutants, resulting in the lowest pollutant

concentrations. Spring lies between summer and winter, both in terms of meteorological conditions and pollutant levels..

In addition to meteorology, variations in emission sources and different atmospheric conditions may also result in variations in the composition of $PM_{2.5}$. Higher temperatures during summer enhance photochemical oxidation but also promote the evaporation of semi-volatile reducing particulate mass. In contrast, lower winter temperatures favor gas–particle partitioning into the particle phase, stabilizing semi-volatile components and contributing to higher $PM_{2.5}$ concentrations

The majority of C-$PM_{2.5}$ mass was dominated by the NR-$PM_{2.5}$ portion, with the highest levels observed during the winter and autumn period (>85%) and the lowest levels during the summer period (66.3%) (Fig. 1 and Fig. S2). Each species' levels and proportional contribution to $PM_{2.5}$ differed depending on the season and diurnal fluctuations. OA contributed the dominant mass fraction in all seasons, followed by other inorganic species, BC, and other elements. We also observed the distinct diurnal fluctuation for inorganic aerosols and BC each season (Fig. 1(b)).

Organic aerosols (OA) were the dominant constituent of C-$PM_{2.5}$ across all seasons (Fig.1), contributing ~54%-51%in winter (≈114–80.4 μg/m³), ~54% in spring (≈58 μg/m³), and ~40.8 in summer (≈25 μg/m³). Their contribution peaked at ~55.5% in autumn (≈104 μg/m³), largely attributable to post-monsoon agricultural residue burning in the Punjab–Haryana region. On a relative scale, mean OA concentrations during winter and spring were ~2–3 times higher than in summer, while autumn levels were nearly fourfold. Distinct diurnal cycles were observed in all seasons, characterized by a morning peak and a stronger nighttime enhancement, reflecting planetary boundary layer dynamics and elevated local emissions, consistent with previous observations in Delhi (e.g. Bhandari et al., 2020). The dominant OA fraction (40–65% of C- $PM_{2.5}$, corresponding to 24–116 μg/m³) is consistent with earlier findings [11,12,29], underscoring the central role of organics in Delhi's fine particulate pollution.

Black carbon contributed between ~6% and 15% of C-$PM_{2.5}$ depending on season, with the highest fractional contribution in summer (14.5%) and lower values in early winter (5.9%), spring (9.0%), autumn (8.6%), and late winter (9.7%). In terms of mass, BC concentrations peaked in late winter (15.2 μg m^{-3}) and autumn (13.6 μg m^{-3}), followed by early winter (12.5 μg m^{-3}), with lower levels in spring (9.3 μg m^{-3}) and summer (8.8 μg m^{-3}). The elevated wintertime BC reflects increased fossil fuel consumption for domestic heating under stagnant boundary layer conditions.

The diurnal profiles of BC (Fig. 1(b)) exhibited a consistent bimodal pattern across all seasons, with peaks during the morning (07:00–09:00) and evening (19:00–22:00). These peaks coincide with local traffic activity, as also reflected in the NO_x profiles (Fig. S1) and are further influenced by emissions from a nearby roadway (~150 m from the site).

The amplitude of the diurnal cycle varied seasonally. Winter and late winter displayed the highest overall concentrations (~18–22 μg m^{-3} at night) and the strongest evening accumulation, attributable to domestic heating emissions combined with boundary layer suppression. Autumn and spring showed intermediate concentrations (10–15 μg m^{-3}) with discernible peaks, though less pronounced than in winter. Summer exhibited the lowest levels (5–10 μg m^{-3}) and a much flatter diurnal cycle, consistent with stronger vertical mixing and higher boundary layer heights that dilute primary emissions.

Secondary inorganic species (NH_4^+, SO_4^{2-}, NO_3^-, Cl^-) exhibited clear seasonal variability driven by emissions and atmospheric processing (Fig. 1 and Fig. S3). The ammonia neutralization ratio (ANR; molar ratio of NH_4^+ to SO_4^{2-}, NO_3^-, and Cl^-) remained close to unity in all seasons, indicating that these species were predominantly present as neutralized salts (NH_4NO_3, $(NH_4)_2SO_4$, and NH_4Cl).

Ammonium showed the lowest concentrations in summer (4.5 μg/m^3, 7.4% of C-$PM_{2.5}$) and increased in spring (9.5 μg/m^3, 9.1%), autumn (14.1 μg/m^3, 8.9%), late winter (20.7 μg/m^3, 13.2%), and peaked in early winter (22.0 μg/m^3, 10.5%). Nitrate dominated the SIA burden in cold months, reaching 28.6 μg/m^3 (13.6%) in early winter and 14.6 μg/m^3 (9.3%) in late winter, compared with 9.6 μg/m^3 (6.0%) in autumn, 7.9 μg/m^3 (7.6%) in spring, and only 2.5 μg/m^3 (4.1%) in summer. Thus, wintertime NO_3^- levels were about ten times higher than in summer.

Sulfate exhibited similar enhancement, with mean concentrations of 23.4 μg/m^3 (11.1%) in early winter, 12.8 μg/m^3 (8.2%) in late winter, 10.4 μg/m^3 (10.0%) in spring, and 7.9 μg/m^3 (5.0%) in autumn, compared with just 4.2 μg/m^3 (6.9%) in summer. Polar plot analysis (Fig. S8) indicated sulfate maxima under easterly flows, consistent with emissions from coal-fired power plants. Stable winter meteorology (low wind speed, low temperature, high RH) further facilitated sulfate accumulation, consistent with aqueous-phase oxidation pathways [30]. Chloride showed weaker seasonal variation, with the highest concentrations in late winter (7.5 μg/m^3, 4.8%) and early winter (5.9 μg/m^3, 2.8%), compared to much lower levels in spring (3.6 μg/m^3, 3.5%), summer (4.5 μg/m^3, 7.4%), and autumn (3.1 μg/m^3, 2.0%).

Elemental mass peaked during summer (11.4 μg/m^3, 18.8%), highlighting the influence of dust storms, while lower contributions were observed in early winter (3.3 μg/m^3, 1.6%), spring (6.6 μg/m^3, 6.3%), autumn (6.9 μg/m^3, 4.3%), and late winter (5.2 μg/m^3, 3.3%). The summer maximum underscores the strong impact of crustal dust on Delhi's aerosol burden (see Section 3.3).

The diurnal patterns of individual aerosol components exhibited strong contrasts between primary and secondary species (Fig. 1(b)). Sulfate displayed relatively stable concentrations throughout the day, with slightly elevated levels during the daytime, particularly in spring and late winter. This enhancement is likely

associated with enhanced photochemical oxidation and the long-range transport of secondary sulfate, as also suggested previous study [29]. The diurnal cycles of nitrate and ammonium were strongly coupled (Fig.1(b)), both showing slight morning peaks between 09:00–11:00 h, followed by a sharp decrease in daytime concentrations. This decline reflects the semi-volatile nature of NH_4NO_3, which undergoes partitioning to the gas phase at elevated temperatures and is further diluted by vertical mixing [31,32].

Chloride exhibited a distinct early-morning maximum (05:00–10:00 h) (Fig.1(b)), after which concentrations decreased rapidly and remained at low stable levels during the rest of the day. This behavior is consistent with the higher vapor pressure of NH_4Cl compared to NH_4NO_3, leading to stronger volatilization at elevated daytime temperatures (Manchanda et al., 2022). Additionally, the rise of the boundary layer after sunrise accelerates the dilution of particulate chloride. While both Cl^- and NO_3^- are semi-volatile, their diurnal evolution differs due to concurrent daytime photochemical oxidation of NO_x to NO_3^-, which partially compensates for its volatilization losses.

3.2. Source apportionment of organic aerosol (OA)

Source apportionment of OA was performed through Rolling PMF window approach to gain insights into the effect sources of OA [25] . PMF on OA aerosols deconvoluted into five factors. The factors were resolved and identified on the basis of distinct spectral signals in specific factors (Fig. 2(c). The temporal variation of the resolved factor was correlated with the external tracers. More details are discussed in the supplementary section S2.

The factors resolved in the current analysis are HOA, BBOA-fresh and BBOA-aged, MO-OOA, and LO-OOA. The HOA factor profile is characterized by the distinct signals of primary alkyl fragments (C_xH_y groups) at m/z 27, 41, 43, 55, 57, 69 and 71. BBOA (fresh) (distinct signals of m/z 60 and m/z 73) . BBOA (Aged) (less m/z 60 and also m/z 44) . OOA factors are characterized by the distinct signals of the m/z 43 and m/z 44 ($C_2H_3O^+$ and CO_2^+). Details regarding each factor's temporal and diurnal variation in different seasons are discussed below (Fig. 2, Fig. S4).

3.2.1 Primary organic factors (POA)

POA was separated into three factors: hydrocarbon-like OA (HOA), biomass burning OA Fresh (BBOA-Fresh), and biomass burning OA Aged (BBOA-Aged). Together, these represent the dominant primary organic sources in Delhi. The HOA concentration exhibited clear seasonal variability (Fig. 2 and Fig. S4), ranging from 13.5 μg/m³ in early Winter to 10.3 μg/m³ in Spring, with intermediate values in, Autumn (7.1 μg/m³), and Late Winter (7.6 μg/m³) and lowest in Summer (4.8 μg/m³). HOA exhibited consistent positive correlations with BC_{ff} across all seasons (r = 0.58–0.82), supporting its identification as a fossil-fuel-

dominated primary aerosol associated with traffic emissions. The strongest association was observed in spring (r = 0.82), while moderate correlations were found in early winter (r = 0.63), late winter (r = 0.61), summer (r = 0.59), and autumn (r = 0.58). HOA displayed two distinct diurnal peaks (Fig. 2(b) in the morning and evening, linked to traffic rush hours. The timing of the evening peak shifted seasonally, occurring later in summer than in winter, consistent with the variation in sunset times and vertical dilution conditions. During daytime hours, HOA exhibited minima across all seasons, reflecting reduced traffic intensity and enhanced boundary layer mixing. The high m/z 55:57 ratio (~1.4) further indicated contributions from cooking emissions, suggesting that HOA in Delhi represents a mixture of traffic and cooking-related sources. Polar plots (Fig. S8) supported its largely local origin across all seasons.

BBOA demonstrated even more pronounced seasonal fluctuations (Fig. 2 and Fig. S4). BBOA-Fresh concentrations increased more than six-fold from 3.3 μg/m³ in Summer to 18.1 μg/m³ in Winter, while its contribution to OA rose from 12% in Summer to 21% in Winter. This highlights the strong role of domestic heating emissions during cold months. The fraction of BBOA decreased rapidly to 7% during Spring, reflecting the reduced need for heating and enhanced atmospheric oxidation. Diurnal patterns of BBOA-Fresh (Fig. 2(b)) showed maxima from the evening to early morning in all seasons, with the strongest nighttime enhancements during Winter. This behaviour suggests a combined role of domestic heating and nighttime boundary layer dynamics.

BBOA-Aged, in contrast, exhibited broader nighttime enhancements across all seasons and remained substantial during Summer (14.7 μg/m³) and Autumn (9.8 μg/m³) (Fig. 2 and Fig. S4), despite the absence of local heating. This factor is interpreted as representing aged biomass burning plumes transported regionally, especially during agricultural burning episodes. Indeed, elevated levels of both BBOA-Fresh and BBOA-Aged were observed in mid-April to early May and again from mid-October to November, coinciding with the Rabi and Kharif harvest burning periods.

To further assess the impact of agricultural burning, daily fire counts for India were compared with biomass burning tracers (Fig. S5), including BBOA-Fresh, BBOA-Aged, the Xact-derived elemental biomass burning factor, and BC_{bb} from BC source apportionment. Seasonal correlation patterns revealed distinct behaviours. BBOA-Fresh exhibited moderate correlations with fire counts in early Winter (r = 0.41), Summer (r = 0.70), and Autumn (r = 0.39), reflecting the influence of both local burning and regional plumes. In contrast, BBOA-Aged showed the strongest correlations, with r = 0.72 in both Summer and Autumn, consistent with long-range transported stubble burning plumes. The Xact biomass burning factor correlated with fire counts in Early Winter (r = 0.51), Spring (r = 0.43), and Summer (r = 0.63), highlighting its sensitivity to both local and transported burning. BC_{bb} emerged as the most consistent tracer, maintaining

strong correlations in Autumn (r = 0.65) and Summer (r = 0.58) and moderate correlation in Early Winter (r = 0.53). These patterns confirm that BC_{bb} and BBOA-Aged best capture the regional influence of stubble burning, while BBOA-Fresh and elemental markers reflect a mixture of local and regional burning influences.

To further examine the relationship between the ACSM-derived biomass-burning factors and independent biomass-burning tracers, multiple linear regression (MLR) was performed using BC_{bb} and the Xact-derived biomass-burning factor (K-rich) as predictor variables (Fig. S20). For BBOA-Aged, BC_{bb} was the dominant predictor overall (standardized $\beta = 0.62$, $R^2 = 0.38$) and during Early Winter ($\beta = 0.45$) and Spring ($\beta = 0.65$), indicating that aged biomass-burning aerosol is closely associated with BC from combustion sources. During Summer, however, the Xact biomass-burning factor became the strongest predictor ($\beta = 0.44$), while in Autumn both BCbb ($\beta = 0.39$) and the Xact biomass-burning factor ($\beta = 0.36$) contributed comparably, consistent with enhanced agricultural residue burning during the Rabi and Kharif burning seasons. In contrast, BBOA-Fresh exhibited a stronger dependence on the Xact biomass-burning factor in early Winter ($\beta = 0.48$), whereas both BC_{bb} and the Xact biomass-burning factor contributed during Spring and Summer. During Autumn, BC_{bb} became the dominant predictor ($\beta = 0.85$), while the negative coefficient associated with the Xact biomass-burning factor likely reflects variance partitioning between correlated predictor variables rather than a negative physical relationship. Overall, the MLR analysis supports the correlation analysis by demonstrating that BBOA-Aged is more strongly linked to regional biomass-burning emissions represented by BC_{bb}, whereas BBOA-Fresh reflects a combination of local combustion emissions and fresh biomass-burning sources.

The strongest tracer–fire count relationships were observed during the stubble burning seasons of mid-April to early May (Rabi harvest) and late October to mid-November (Kharif harvest). In other seasons, weaker correlations suggest a greater role for local sources and secondary organic aerosol formation. Importantly, while BBOA-Aged peaks coincide with fire counts in late October–November, day-to-day variability and non-biomass contributions limit the strength of the correlation at daily resolution. Overall, these results emphasized that HOA in Delhi is dominated by local traffic and cooking sources, whereas BBOA-Fresh captures short-lived local burning and domestic heating, and BBOA-Aged represents long-range transported plumes. Among all tracers, BC_{bb} and BBOA-Aged provide the clearest signatures of regional biomass burning impacts.

The seasonal PSCF plots (Figs. S12 and S13) indicate that both BBOA-Fresh and BBOA-Aged are influenced by similar regional biomass-burning source areas over the Indo-Gangetic Plain, suggesting a common regional origin. BBOA-Aged generally exhibits a broader and more diffuse spatial probability

distribution than BBOA-Fresh, particularly during the major burning seasons, indicating greater atmospheric aging and transport prior to arrival at the receptor. The two factors are also only moderately correlated ($R^2 \approx 0.25$), suggesting that they represent different stages of atmospheric processing rather than completely independent source regions.

During Autumn, PSCF analyses show enhanced source probabilities extending over Punjab and Haryana, consistent with the Kharif residue-burning region, while summer exhibits elevated probabilities associated with the Rabi burning period across the northwestern Indo-Gangetic Plain. In Early and Late Winter, both factors show contributions from Haryana, Rajasthan and surrounding regions together with local emissions, reflecting the combined influence of residential biomass burning and regional transport under shallow boundary layer conditions. The differences between BBOA-Fresh and BBOA-Aged are therefore primarily reflected in their temporal behavior, diurnal evolution, fire-count correlations, and relationships with independent biomass-burning tracers (BC_{bb} and the Xact-derived biomass-burning factor), rather than fundamentally different geographical source regions.

3.2.2 Oxidized Organic Aerosols (OOA)

Oxidized organic aerosol (OOA) factors dominated the OA mass across all seasons, contributing between 60–90% of total OA (Fig. 2). The seasonal contribution of OOA was highest during Summer and Autumn (≥80% of OA mass), consistent with previous studies in other regions [11,25,33], and relatively lower during Early Winter, Late Winter, and Spring (60–65%).

Two distinct OOA factors were resolved: more-oxidized oxygenated organic aerosol (MO-OOA), characterized by a higher contribution from m/z 44 (CO_2^+), and less-oxidized oxygenated organic aerosol (LO-OOA), characterized by a higher contribution from m/z 43 ($C_2H_3O^+$). MO-OOA reached its highest mean seasonal concentrations in Autumn (65.2 μg/m³) and early Winter (47.5 μg/m³), followed by Late Winter (48.2 μg/m³). The lowest values were observed in Summer (11.4 μg/m^{-3}) and Spring (19.4 μg/m³). LO-OOA followed a similar but weaker pattern, with maxima in Autumn (25.4 μg/m³) and early Winter (21.7 μg/m³), and minima in Summer (5.9 μg/m³) and Spring (12.4 μg/m³).

The Summer and Autumn periods coincide with agricultural harvesting and residue burning, yet the oxidation environments differ significantly. In Summer, high temperatures and elevated ozone promoted rapid photochemical aging, efficiently converting LO-OOA into MO-OOA during daytime. This was reflected in the moderate mean concentrations of both factors and relatively flat diurnal profiles, suggesting a balance between production and dispersion. In Autumn, by contrast, fresh burning emissions coincided

with the accumulation of regionally transported aged OA, yielding the highest contribution of MO-OOA to total OA (59.3%) and strong fire count correlations (r = 0.68 for MO-OOA).

In Early Winter, LO-OOA correlated moderately with BC_{bb} (r = 0.50) (Fig. S7), indicating fresh biomass burning and residential heating emissions. Night-time maxima were particularly enhanced due to shallow boundary layers, nocturnal inversions, and stronger condensation at lower temperatures. MO-OOA in the same season displayed a dual peak structure, with a midday maximum linked to photochemical production and an evening maximum likely related to regional transport and re-condensation. Late Winter showed similar behaviour, but with weaker correlations between LO-OOA and BC_{bb} (r = 0.36) and reduced night-time enhancements, consistent with the gradual decline in heating activities.

Spring was characterized by the lowest oxidized OA concentrations among all seasons (MO-OOA: 19.4 μg/m³, LO-OOA: 12.4 μg/m³) and weak correlations with both BCbb and fire counts. This reflects a shift in dominant sources, with traffic-related SOA and mineral dust contributions outweighing biomass burning. Diurnal variability was muted, with weaker night-time build-up compared to winter, reflecting enhanced vertical mixing and reduced local burning.

Taken together, the results show that LO-OOA is more strongly linked to fresh combustion emissions, particularly during Early Winter and Autumn, while MO-OOA reflects chemically aged OA influenced by both photochemical oxidation and regional transport. Seasonal contrasts between Summer and Autumn demonstrate that while biomass burning is a common source, the oxidation regime and transport conditions critically determine whether freshly emitted OA persists as semi-volatile or is rapidly converted into highly oxidized MO-OOA, which also evident form the PSCF plot (Fig. S14 and Fig. S15)

3.3 Source apportionment of elemental aerosols

Source apportionment of elemental aerosols is deconvoluted into nine sources (Fig. 3a: power plant, dust, biomass burning, vehicular emission, secondary chloride, waste incineration, industrial emissions (Pb-rich and Cu-rich) with an additional factor during the Diwali period in autumn season, fireworks were identified. More than 50% of $PM_{2.5}$ el is dominated by power plant (PP), and secondary chloride (SC),) in all seasons (Fig. 3c), except in the summer and spring seasons, where dust-related sources also contribute significantly to $PM_{2.5}$ el SA as multiple dust storms are observed in the summer seasons. Details regarding the temporal and diurnal variation (Fig. 3 and Fig. S6) of these factors in different seasons are discussed below

3.3.1 Power plant, Biomass burning, and Secondary chloride

Power Plant

The power plant factor was characterized by a dominant sulfur signature, with notable contributions from trace elements such as As, Se, and Ba. This factor showed marked seasonal variability, with the highest contributions during the winter months. In late winter, the power plant factor reached 6.2 μg/m³ (35.0%), while in early winter it contributed 4.7 μg/m³ (33.0%). Contributions were lower in spring (2.9 μg/m³, 21.6%) and autumn (3 μg/m³, 23.0%), and reached a seasonal minimum in summer (1.9 μg/m³, 10.5%). The enhanced wintertime contribution is consistent with more efficient SO_2-to-SO_4^{2-} conversion under cold, humid, and stagnant meteorological conditions.

In terms of diurnal variation, the sulfur-rich factor did not exhibit a pronounced diurnal cycle, with only a slight daytime enhancement, consistent with the behavior of sulfate (Fig. 3b). This daytime increase is attributed to the photochemical oxidation of SO_2 to secondary sulfate [29] . The PSCF analysis (Fig. S16) indicated that elevated concentrations were associated with air masses arriving from the east and southeast of the sampling site. This observation is consistent with satellite-based emission studies [34], which identify the eastern and southeastern sectors surrounding Delhi, including the NTPC Dadri thermal power station, as major SO_2 emission hotspots associated with coal-fired power generation. Consequently, the sulfur-rich factor is primarily attributed to secondary sulfate formed from SO_2 emissions originating from regional coal-fired thermal power plants.

Biomass burning

The biomass burning (BB) factor was characterized by high potassium (K) contributions, consistent with its widespread use as an elemental tracer for biomass combustion sources [35–38]. Biomass burning exhibited variable contributions across seasons, with the highest fractions in summer (1.3 μg/m³, 7.3%), followed by autumn (1.1 μg/m³, 8.7%). Lower contributions were observed in spring (0.9 μg/m³, 6.6%), early (0.5 μg/m³, <5.%) and late winter (0.9 μg/m³, < 5%). The summer BB period coincided with stubble burning activities in the northwest region, further amplifying its influence on ambient $PM_{2.5}$ levels.

The diurnal cycle of the BB factor showed a consistent bimodal pattern, with a distinct morning peak and a stronger nocturnal enhancement across all seasons (Fig. 3(b)). The dominance of nighttime contributions indicates modulation by boundary layer height dynamics, with shallow nocturnal boundary layers trapping BB emissions near the surface. This diurnal behavior is in close agreement with the biomass burning organic aerosol (BBOA) factor identified in the OA-PMF analysis, both showing reduced contributions during the winter-to-spring transition.

Secondary chloride

The Cl-rich factor was consistently dominated by chlorine across all seasons, confirming chloride as its defining tracer. The factor contributed most during late winter (7.5 μg/m³, 42.2%) and early winter (6.4 μg/m³, 44.7%), whereas lower contributions were observed during spring (3.7 μg m^{-3}, 27.6%), summer (4.7 μg/m³, 26.4%), and autumn (3.1 μg/m³, 24.5%). The enhanced wintertime abundance is consistent with

reduced boundary layer height and meteorological conditions that favor the accumulation of particulate chloride.

The diurnal profile (Fig. 3b) exhibited pronounced nighttime maxima and daytime minima across all seasons. This behavior is consistent with the volatilization of semi-volatile ammonium chloride under warmer daytime conditions together with dilution associated with enhanced daytime boundary layer development. However, the weaker daytime decrease observed during late winter suggests that lower temperatures and higher relative humidity favor the thermodynamic stability of particulate chloride, reducing its volatilization. Moreover, the observed temporal pattern alone does not necessarily imply that the resolved factor is exclusively secondary. Previous studies have shown that particulate chloride in Delhi originates from multiple sources, including biomass burning, coal combustion, industrial emissions, and open waste burning, particularly the combustion of chlorine-containing materials such as PVC, in addition to secondary formation through the reaction of gaseous HCl with ammonia [19,29,30,39].

The PSCF analysis (Fig. S17) further indicates enhanced source probabilities over the northwestern sector, consistent with previous observations linking elevated chloride concentrations to regional transport from industrial regions and biomass-burning emissions. Consequently, the Cl-rich factor is more appropriately interpreted as representing a combination of primary chloride emissions and secondary chloride formation rather than a purely secondary aerosol source.

3.3.2 Metal dominated factors Industrial (Cu rich), Pb rich and waste incineration (Zn –rich)

Industrial, Waste Incineration, and Pb-rich Source Contributions

The industrial (Cu-rich) factor was consistently dominated by Cu across all seasons, in agreement with previous work identifying Cu as a robust tracer for industrial emissions in Delhi [19]. Cu contributions remained relatively small, ranging between 0.1–0.3 μg/m³ (1–2% of total elemental $PM_{2.5}$). This source is likely related to emissions from electrical and electronic equipment recycling and processing, which contain substantial amounts of copper [40,41]. The waste incineration factor, dominated by Zn, showed stable contributions throughout the year (0.4–0.5 μg/m³, ~2–4%). Zn has been widely associated with emissions from waste incineration processes as well as the iron and steel industries [19,42]. The Industrial (Pb-rich) factor, dominated by Pb, contributed ~1.0 μg/m³ in Early Winter, Autumn, and Late Winter, slightly lower in Spring (0.9 μg/m³), and reached a minimum in Summer (0.5 μg/m³). Pb is a well-established marker of steel and pigment production, lead-acid battery manufacturing and recycling, and non-ferrous metal smelting [14,43].

The polar plots (Fig. S9, S10, S11) provide further insight into the directional and meteorological influences governing these sources. The Cu-rich industrial factor displayed elevated concentrations under moderate wind speeds (1–2 m/s) from the southwest to west, particularly during Early and Late Winter, suggesting contributions from nearby industrial estates and small-scale metal processing facilities situated upwind of Delhi. During Summer, enhanced Cu signals were occasionally observed under easterly flow, likely reflecting shifts in synoptic circulation and daytime boundary layer mixing.

The Zn-rich waste incineration factor showed the highest intensities during Autumn and Late Winter, under northerly to northwesterly winds, consistent with emissions from municipal and industrial waste burning along Delhi's northern periphery. Broader angular distributions in Spring and Summer indicate additional influence from scattered open waste burning and small industrial sources within the city.

The Pb-rich factor exhibited distinct hotspots under low wind speeds (<1.5 m/s) and northwesterly flow during Early Winter, Autumn, and Late Winter, pointing to local metallurgical and battery recycling activities within Delhi and nearby clusters in Ghaziabad and Faridabad. During Spring and Summer, moderate Pb-rich concentrations appeared under easterly flow, suggesting a partial contribution from regional transport.

Collectively, these metal-dominated sources accounted for approximately 10–15% of total elemental $PM_{2.5}$. Their nocturnal enhancement and association with low wind speeds imply predominantly local origin and nighttime accumulation under shallow boundary layers, in agreement with the diurnal trends observed (Fig. 3b). The seasonal directionality and wind-dependence captured by the polar plots further confirm the persistent influence of industrial and waste-related activities on Delhi's elemental aerosol composition.

3.3.3 Dust-related and Traffic-related Source

The dust-related factor was characterized by high loadings of crustal elements (Si, Ca, Ti, and Fe), consistent with their established role as tracers of crustal and road dust [44]. This factor showed pronounced seasonal variability, with enhanced contributions during spring and summer relative to winter and autumn. Its maximum contribution occurred during summer (8.1 μg m^{-3}, 45%), followed by spring (3.6 μg m^{-3}, 27%), whereas substantially lower contributions were observed during early winter (0.6 μg m^{-3}, 3.4%), late winter (0.7 μg m^{-3}, 3.7%), and autumn (1.5 μg m^{-3}, 11.5%). The enhanced summer contribution reflects both regional dust transport and local resuspension, further amplified by dust storm events observed in late April (Fig. S6), consistent with previous observations in Delhi [14]. Since XACT quantifies elemental concentrations rather than their oxide forms, the reported dust factor represents only the elemental fraction

of mineral aerosol. To illustrate the magnitude of this underestimation, we reconstructed the mineral oxide mass for the summer period following the improve mineral reconstruction approach [45]. The reconstructed mineral mass increased from 8.1 to approximately 17.3 μg m^{-3}, demonstrating that the elemental dust factor substantially underestimates the total mineral aerosol burden because oxygen associated with mineral oxides is not directly measured.

The diurnal cycle of the dust-related factor displayed two peaks: one in the afternoon (linked to enhanced turbulence-driven resuspension) and another at night, attributed to resuspension from heavy-duty vehicle (HDV) activity permitted during nighttime hours.

The traffic-related factor was enriched in Cr and Mn, elements commonly associated with vehicular tailpipe emissions, brake wear, and engine wear [43]. Seasonal contributions remained modest but persistent across all seasons, ranging from 0.5–1.3 μg/m^3 (3–7%), with the maximum contribution observed in summer (1.3 μg/m^3, 7.3%). Its diurnal variation showed distinct morning and evening rush-hour peaks (Fig. 3(b)), consistent with local traffic activity near the site.

The fossil fuel fraction of BC (BC_{ff}) exhibited variable correlation with traffic-related tracers (Fig. S7). Spring showed the strongest associations between the traffic metals factor dominated by Cr, Mn, Fe, Ni, and Zr (r = 0.61), indicating vehicular emissions as the dominant BC source. In early winter (January–mid February), correlations weakened (r = 0.27), likely due to additional fossil fuel contributions from residential heating and coal/oil combustion. Autumn and summer displayed moderate correlations, while late winter (December) exhibited higher associations (traffic metals: r = 0.53; HOA) than early winter, reflecting stable atmospheric conditions, across seasons.

4. Conclusions

This study provides a seasonally resolved, composition-integrated characterization of $PM_{2.5}$ in Delhi using concurrent high-time-resolution measurements of non-refractory species, elements, and black carbon. Strong seasonal variability was observed, with maximum concentrations during early and late winter and autumn, driven by shallow boundary layers, high relative humidity, and enhanced regional transport, and minimum levels in summer due to efficient atmospheric dispersion.

Organic aerosol dominated $PM_{2.5}$ mass (40–65%) across all seasons. Rolling PMF resolved five OA factors (HOA, BBOA-Fresh, BBOA-Aged, LO-OOA, and MO-OOA), highlighting the coexistence of local primary emissions and regionally transported aged aerosol. HOA reflected traffic and cooking sources with pronounced bimodal diurnal cycles. Biomass burning showed distinct signatures, with BBOA-Fresh

associated with local combustion and heating, and BBOA-Aged strongly linked to regional agricultural residue burning. Oxidized OA constituted 60–90% of total OA, indicating the dominant role of secondary organic aerosol formation. Seasonal contrasts revealed enhanced photochemical aging in summer and combined transport–accumulation effects in autumn and winter.

Secondary inorganic aerosols were strongly enhanced during winter, with nitrate and sulfate driven by thermodynamic partitioning and regional coal-fired power plant emissions, respectively. Secondary chloride exhibited pronounced nocturnal accumulation consistent with semi-volatile behavior. Elemental PMF identified nine sources, including power plants, dust, biomass burning, traffic, secondary chloride, industrial and waste-related metals, and episodic fireworks during Diwali. Dust dominated in summer, while sulfur-rich power plant emissions and secondary formation processes governed winter pollution.

Overall, Delhi's $PM_{2.5}$ burden reflects the combined effects of local emissions, regional transport, and intensive secondary processing. The predominance of secondary and regionally influenced components underscores the need for coordinated, multi-sectoral mitigation strategies targeting precursor emissions across the Indo-Gangetic Plain.

Acknowledgements

The authors acknowledge funding from the Swiss Agency for Development and Cooperation (SDC) through the Clean Air Project in India (Grant No. 7F-10093.01.04) and the Consolidation Phase of the Clean-Air-China Programme (Grant No. 7F-09802.01.03). The authors also acknowledge the Indian Institute of Technology Delhi (IIT Delhi) for financial support through the IRD Grand Challenge Project (Grant No. IITD/IRD/MI01810G).

References:

1. WHO. *WHO's Urban Ambient Air Pollution Database-Update 2016 Version 0.2*. https://cdn.who.int/media/docs/default-source/air-quality-database/aqd-2016/aap_database_methods_2016_v03.pdf?sfvrsn=b71455b4_3 (2016).

2. Mahato, S., Pal, S. & Ghosh, K. G. Effect of lockdown amid COVID-19 pandemic on air quality of the megacity Delhi, India. *Science of the Total Environment* **730**, (2020).

3. WHO. *WHO Ambient (Outdoor) Air Quality Database*. https://cdn.who.int/media/docs/default-source/air-quality-database/aqd-2018/aap_database_summary_results_2018_final2.pdf?sfvrsn=7b92eafc_3 (2018).

4. Heal, M. R., Kumar, P. & Harrison, R. M. Particles, air quality, policy and health. *Chem. Soc. Rev.* **41**, 6606–6630 (2012).

5. Dholakia, H. H., Purohit, P., Rao, S. & Garg, A. Impact of current policies on future air quality and health outcomes in Delhi, India. *Atmos. Environ.* **75**, 241–248 (2013).

6. Pant, P. *et al.* Characterization of ambient PM2.5 at a pollution hotspot in New Delhi, India and inference of sources. *Atmos. Environ.* **109**, 178–189 (2015).

7. Jain, S., Sharma, S. K., Mandal, T. K. & Saxena, M. Source apportionment of PM10 in Delhi, India using PCA/APCS, UNMIX and PMF. *Particuology* **37**, 107–118 (2018).

8. Nagar, P. K. *et al.* Characterization of PM2.5 in Delhi: role and impact of secondary aerosol, burning of biomass, and municipal solid waste and crustal matter. *Environmental Science and Pollution Research* **24**, 25179–25189 (2017).

9. Sharma, H., Jain, V. K. & Khan, Z. H. Characterization and source identification of polycyclic aromatic hydrocarbons (PAHs) in the urban environment of Delhi. *Chemosphere* **66**, 302–310 (2007).

10. Rai, P. *et al.* Source apportionment of highly time-resolved elements during a firework episode from a rural freeway site in Switzerland. *Atmos. Chem. Phys.* **20**, 1657–1674 (2020).

11. Tobler, A. *et al.* Chemical characterization of PM2.5 and source apportionment of organic aerosol in New Delhi, India. *Science of the Total Environment* **745**, 1–12 (2020).

12. Cash, J. M. *et al.* Seasonal analysis of submicron aerosol in Old Delhi using high-resolution aerosol mass spectrometry: Chemical characterisation, source apportionment and new marker identification. *Atmos. Chem. Phys.* **21**, 10133–10158 (2021).

13. Manchanda, C. *et al.* Variation in chemical composition and sources of PM2.5 during the COVID-19 lockdown in Delhi. *Environ. Int.* **153**, 106541 (2021).

14. Shukla, A. K. *et al.* Spatio-temporal variation of C-PM2.5 (composition based PM2.5) sources using PMF*PMF (double-PMF) and single-combined PMF technique on real-time non-refractory, BC and elemental measurements during post-monsoon and winter at two sites in Delhi, India. *Atmos. Environ.* **293**, 119456 (2023).

15. Faisal, M., Ali, U., Kumar, A., Kumar, M. & Singh, V. Unveiling PM2.5 sources: Double and tracer conjugate PMF approaches for high-resolution organic, BC, and inorganic PM2.5 data. *Atmos. Environ.* **343**, (2025).

16. Faisal, M., Hazarika, N., Ganguly, D., Kumar, M. & Singh, V. PM2.5 bound species variation and source characterization in the post-lockdown period of the Covid-19 pandemic in Delhi. *Urban Clim.* **46**, (2022).

17. Kumar, A. *et al.* Two different approaches for source apportionment of ambient black carbon in highly polluted environments. *Atmos. Environ.* **338**, 120863 (2024).

18. Bhandari, S. *et al.* Sources and atmospheric dynamics of organic aerosol in New Delhi, India: Insights from receptor modeling. *Atmos. Chem. Phys.* **20**, 735–752 (2020).

19. Faisal, M., Hazarika, N., Ganguly, D., Kumar, M. & Singh, V. PM2.5 bound species variation and source characterization in the post-lockdown period of the Covid-19 pandemic in Delhi. *Urban Clim.* **46**, 101290 (2022).

20. Faisal, M., Ali, U., Kumar, A., Kumar, M. & Singh, V. Unveiling PM2.5 sources: Double and tracer conjugate PMF approaches for high-resolution organic, BC, and inorganic PM2.5 data. *Atmos. Environ.* **343**, (2025).

21. Rai, P. *et al.* Real-time measurement and source apportionment of elements in Delhi's atmosphere. *Science of the Total Environment* **742**, 140332 (2020).

22. Goel, V. *et al.* Ambient black carbon and its dependence on in situ stubble burning. *Environ. Monit. Assess.* **198**, (2026).

23. Paatero, P., Eberly, S., Brown, S. G. & Norris, G. A. Methods for estimating uncertainty in factor analytic solutions. *Atmos. Meas. Tech.* **7**, 781–797 (2014).

24. Chen, F. & Dudhia, J. *Coupling an Advanced Land Surface-Hydrology Model with the Penn State-NCAR MM5 Modeling System. Part I: Model Implementation and Sensitivity*.

25. Chen, G. *et al.* European aerosol phenomenology − 8: Harmonised source apportionment of organic aerosol using 22 Year-long ACSM/AMS datasets. *Environ. Int.* **166**, (2022).

26. Canonaco, F. *et al.* A new method for long-term source apportionment with time-dependent factor profiles and uncertainty assessment using SoFi Pro: Application to 1 year of organic aerosol data. *Atmos. Meas. Tech.* **14**, 923–943 (2021).

27. Kumar, A. *et al.* Two different approaches for source apportionment of ambient black carbon in highly polluted environments. *Atmos. Environ.* **338**, (2024).

28. Sun, Y. L. *et al.* Aerosol composition, sources and processes during wintertime in Beijing, China. *Atmos. Chem. Phys.* **13**, 4577–4592 (2013).

29. Gani, S. *et al.* Submicron aerosol composition in the world's most polluted megacity: The Delhi Aerosol Supersite study. *Atmos. Chem. Phys.* **19**, 6843–6859 (2019).

30. Ali, U., Faisal, M., Ganguly, D., Kumar, M. & Singh, V. Analysis of aerosol liquid water content and its role in visibility reduction in Delhi. *Science of the Total Environment* **867**, 161484 (2023).

31. HARRISON, R. M. & PIO, C. A. An investigation of the atmospheric HNO3–NH3–NH4NO3 equilibrium relationship in a cool, humid climate. *Tellus B* **35 B**, 155–159 (1983).

32. Ali, U., Faisal, M., Ganguly, D., Kumar, M. & Singh, V. Analysis of aerosol liquid water content and its role in visibility reduction in Delhi. *Science of the Total Environment* **867**, (2023).

33. Via, M., Minguillón, M. C., Reche, C., Querol, X. & Alastuey, A. Increase in secondary organic aerosol in an urban environment. *Atmos. Chem. Phys.* **21**, 8323–8339 (2021).

34. Ghosh, S. *et al.* Air quality and health benefits achievable by mitigating Indian coal-fired power plant SO2 emissions. *npj Clean Air* **2**, (2026).

35. Khare, P. & Baruah, B. P. Elemental characterization and source identification of PM2.5 using multivariate analysis at the suburban site of North-East India. *Atmos. Res.* **98**, 148–162 (2010).

36. Shridhar, V., Khillare, P. S., Agarwal, T. & Ray, S. Metallic species in ambient particulate matter at rural and urban location of Delhi. *J. Hazard. Mater.* **175**, 600–607 (2010).

37. Pant, P. & Harrison, R. M. Critical review of receptor modelling for particulate matter: A case study of India. *Atmospheric Environment* vol. 49 1–12 Preprint at https://doi.org/10.1016/j.atmosenv.2011.11.060 (2012).

38. Reche, C. *et al.* Real-time indoor and outdoor measurements of black carbon at primary schools. *Atmos. Environ.* **120**, 417–426 (2015).

39. Manchanda, C., Kumar, M. & Singh, V. Meteorology governs the variation of Delhi's high particulate-bound chloride levels. *Chemosphere* **291**, (2022).

40. Frazzoli, C., Orisakwe, O. E., Dragone, R. & Mantovani, A. Diagnostic health risk assessment of electronic waste on the general population in developing countries' scenarios. *Environ. Impact Assess. Rev.* **30**, 388–399 (2010).

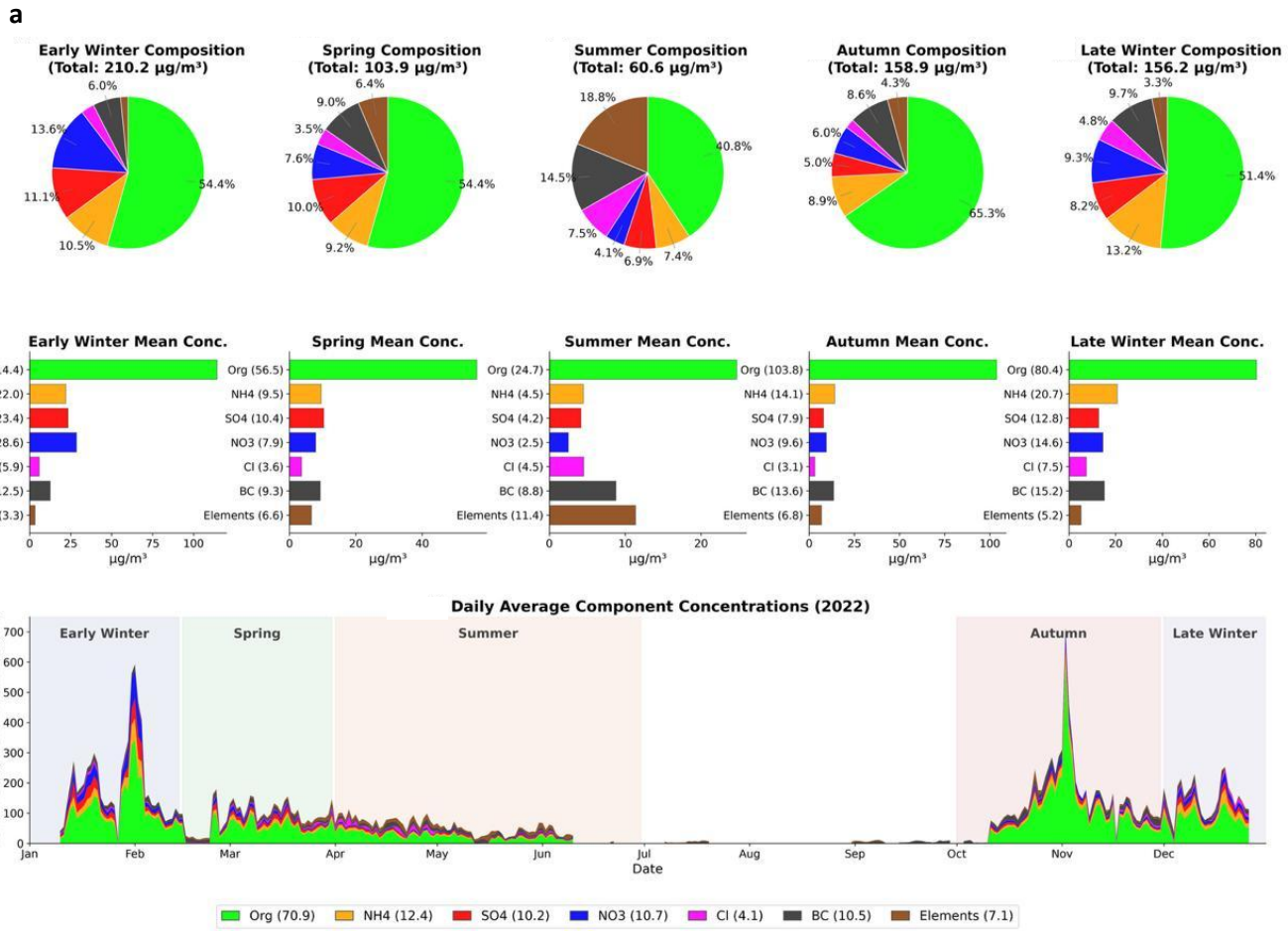
41. Owoade, K. O. *et al.* Chemical compositions and source identification of particulate matter (PM2.5 and PM2.5–10) from a scrap iron and steel smelting industry along the Ife–Ibadan highway, Nigeria. *Atmos. Pollut. Res.* **6**, 107–119 (2015).

42. Duan, J. & Tan, J. Atmospheric heavy metals and Arsenic in China: Situation, sources and control policies. *Atmospheric Environment* vol. 74 93–101 Preprint at https://doi.org/10.1016/j.atmosenv.2013.03.031 (2013).

43. Jeong, C.-H., Wang, J. M. & Evans, G. J. Source Apportionment of Urban Particulate Matter using Hourly Resolved Trace Metals, Organics, and Inorganic Aerosol Components. Preprint at https://doi.org/10.5194/acp-2016-189 (2016).

44. Gupta, A. K., Karar, K. & Srivastava, A. Chemical mass balance source apportionment of PM10 and TSP in residential and industrial sites of an urban region of Kolkata, India. *J. Hazard. Mater.* **142**, 279–287 (2007).

45. Chow, J. C., Lowenthal, D. H., Chen, L. W. A., Wang, X. & Watson, J. G. Mass reconstruction methods for PM2.5: a review. *Air Qual. Atmos. Health* **8**, 243–263 (2015).


a
Early Winter Composition
(Total: 210.2 µg/m³)
6.0%
13.6%
11.1%
10.5%
54.4%
Spring Composition
(Total: 103.9 µg/m³)
6.4%
9.0%
3.5%
7.6%
10.0%
9.2%
54.4%
Summer Composition
(Total: 60.6 µg/m³)
18.8%
40.8%
14.5%
7.5%
4.1%
6.9%
7.4%
Autumn Composition
(Total: 158.9 µg/m³)
4.3%
8.6%
6.0%
5.0%
8.9%
65.3%
Late Winter Composition
(Total: 156.2 µg/m³)
3.3%
9.7%
4.8%
9.3%
8.2%
13.2%
51.4%
Early Winter Mean Conc.
Org (114.4)
NH4 (22.0)
SO4 (23.4)
NO3 (28.6)
Cl (5.9)
BC (12.5)
Elements (3.3)
µg/m³
Spring Mean Conc.
Org (56.5)
NH4 (9.5)
SO4 (10.4)
NO3 (7.9)
Cl (3.6)
BC (9.3)
Elements (6.6)
µg/m³
Summer Mean Conc.
Org (24.7)
NH4 (4.5)
SO4 (4.2)
NO3 (2.5)
Cl (4.5)
BC (8.8)
Elements (11.4)
µg/m³
Autumn Mean Conc.
Org (103.8)
NH4 (14.1)
SO4 (7.9)
NO3 (9.6)
Cl (3.1)
BC (13.6)
Elements (6.8)
µg/m³
Late Winter Mean Conc.
Org (80.4)
NH4 (20.7)
SO4 (12.8)
NO3 (14.6)
Cl (7.5)
BC (15.2)
Elements (5.2)
µg/m³
Daily Average Component Concentrations (2022)
Early Winter
Spring
Summer
Autumn
Late Winter
Daily Average Concentration (µg/m³)
Jan
Feb
Mar
Apr
May
Jun
Jul
Aug
Sep
Oct
Nov
Dec
Date
Org (70.9)
NH4 (12.4)
SO4 (10.2)
NO3 (10.7)
Cl (4.1)
BC (10.5)
Elements (7.1)

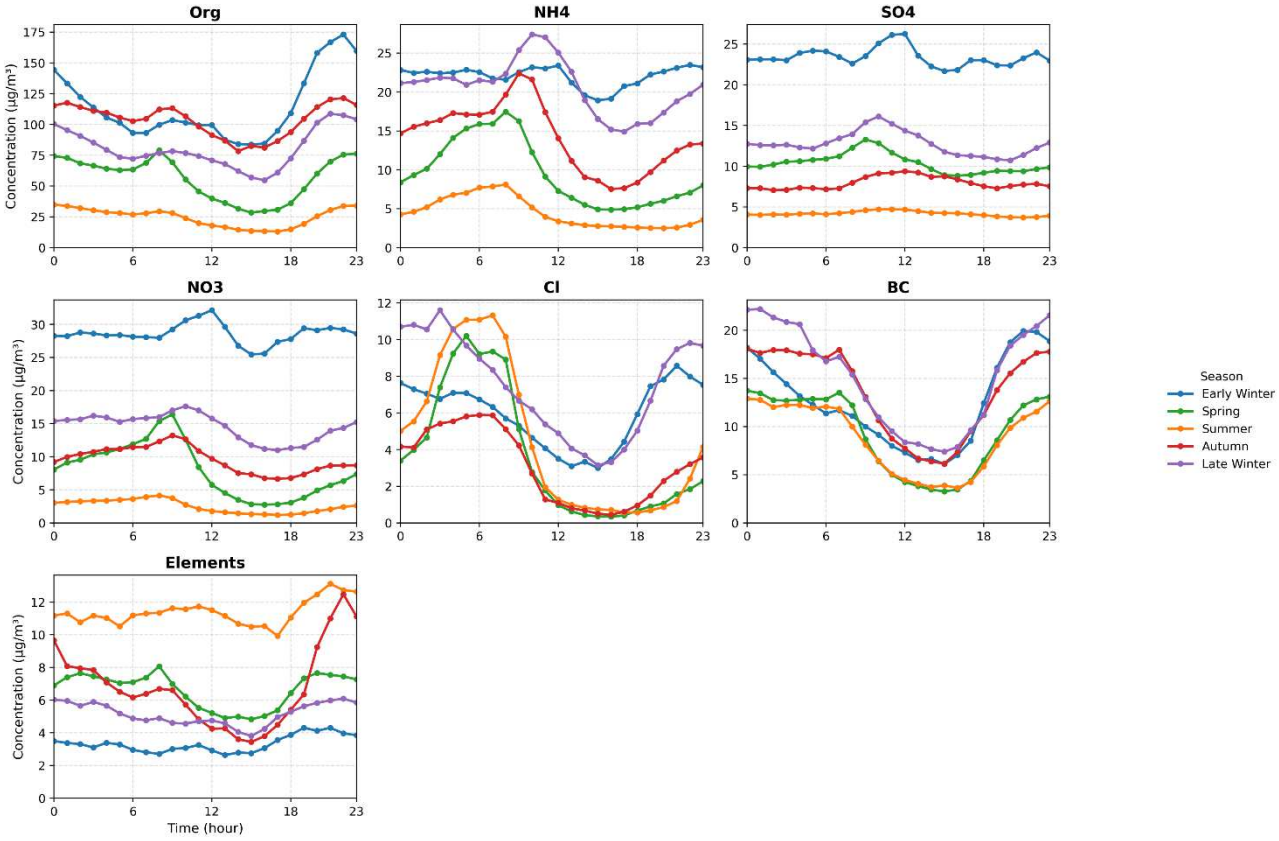
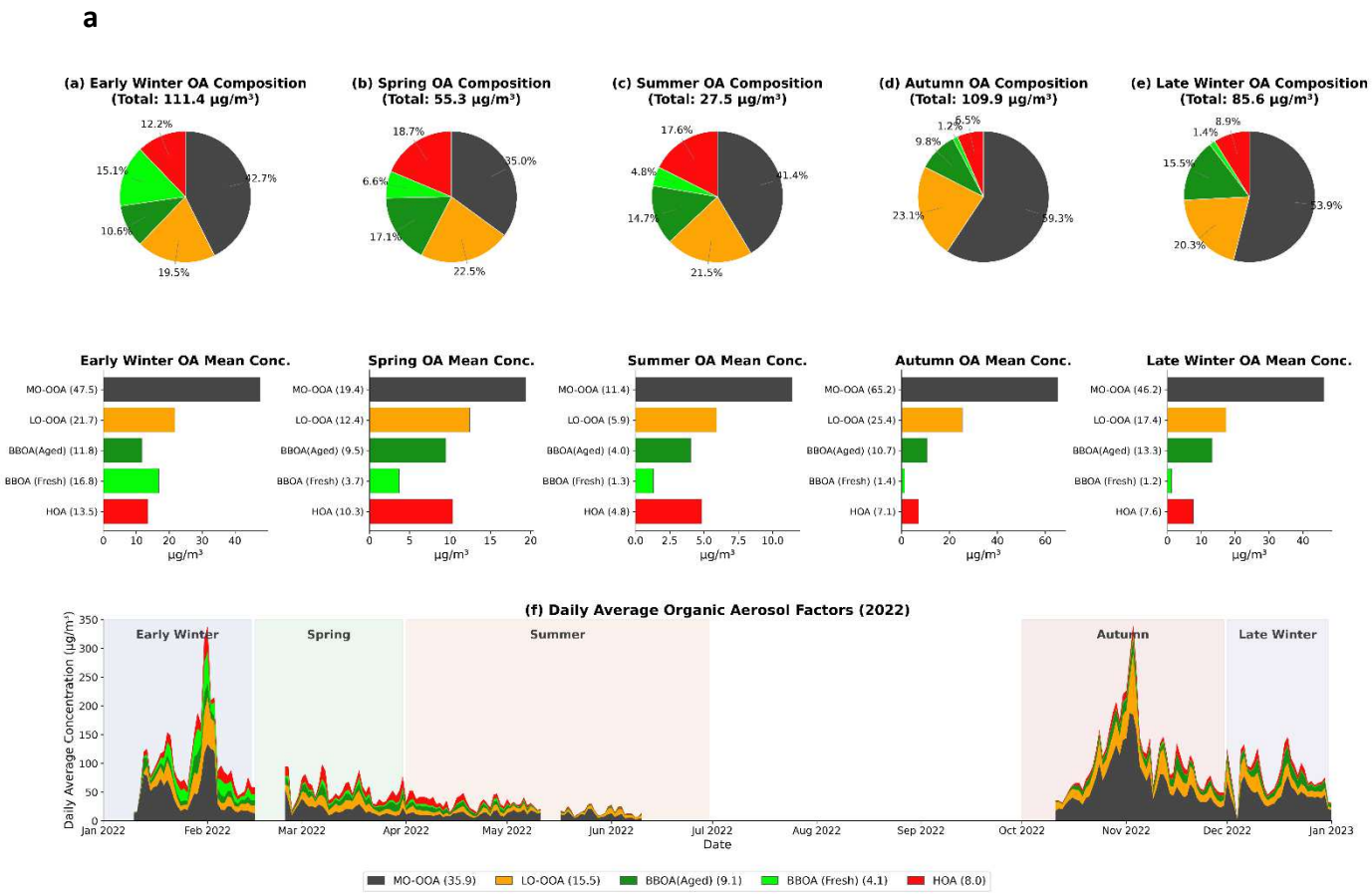
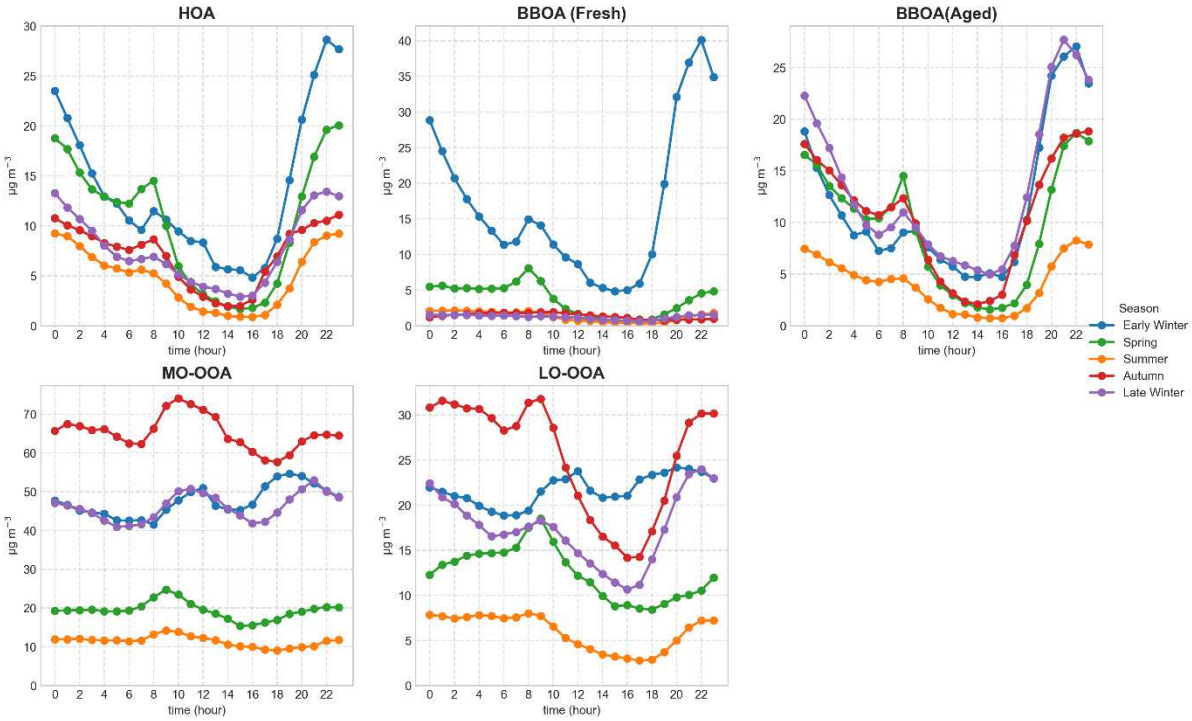
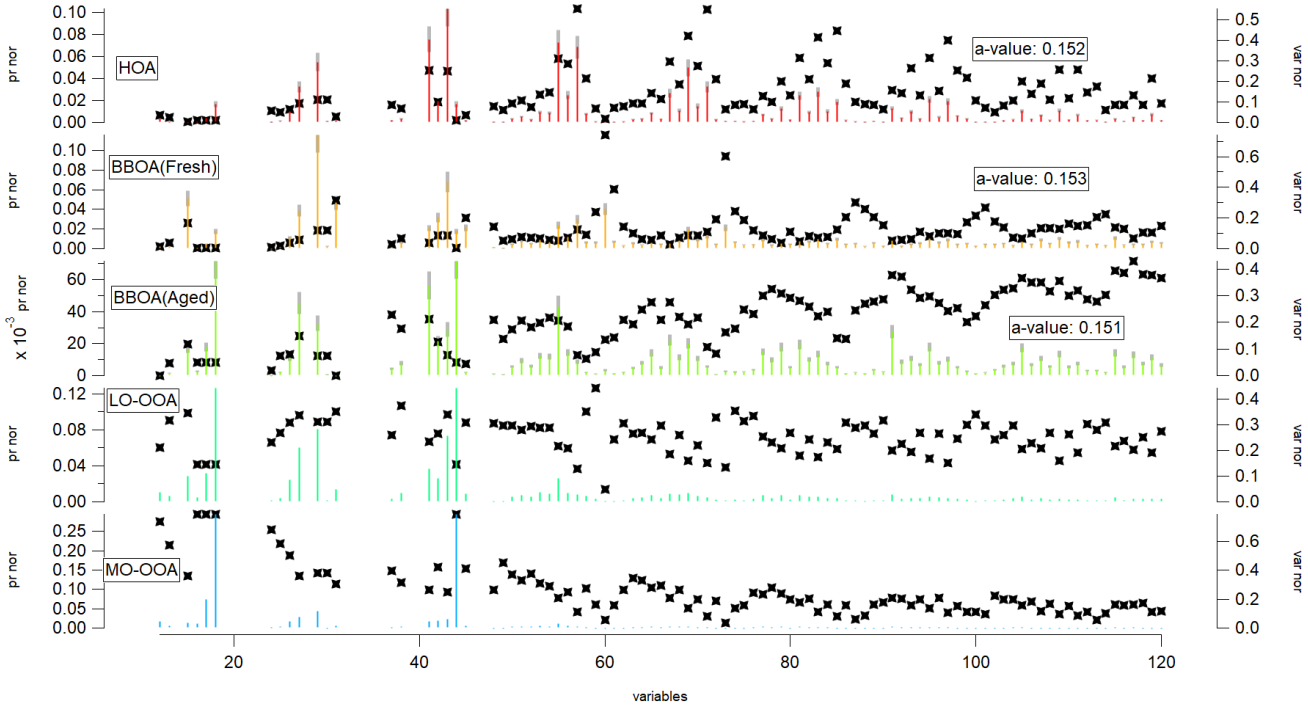

b
Org
NH4
SO4
NO3
Cl
BC
Elements
Concentration (µg/m³)
Time (hour)
Season
Early Winter
Spring
Summer
Autumn
Late Winter

Figure 1. Seasonal composition and diurnal variation of major $PM_{2.5}$ components. (a) Top Panels show pie charts of seasonal mass fractions and bar plots of mean concentrations during Early Winter, Spring, Summer, Autumn, and Late Winter. Organics dominated across all seasons (40–65%), with maximum contributions during autumn, coinciding with post-monsoon crop residue burning. Secondary inorganic aerosols (NH_4^+, SO_4^{2-}, NO_3^-, Cl^-), black carbon, and crustal elements displayed strong seasonal variability, with highest nitrate and ammonium during winter and autumn. Bottom panel illustrates daily average concentrations, highlighting seasonal peaks. (b) Shows diurnal patterns of each component, with strong morning and nighttime enhancements for organics, ammonium, nitrate, chloride, and BC due to boundary layer dynamics and local emissions, while sulfate exhibited daytime maxima driven by photochemistry.



b

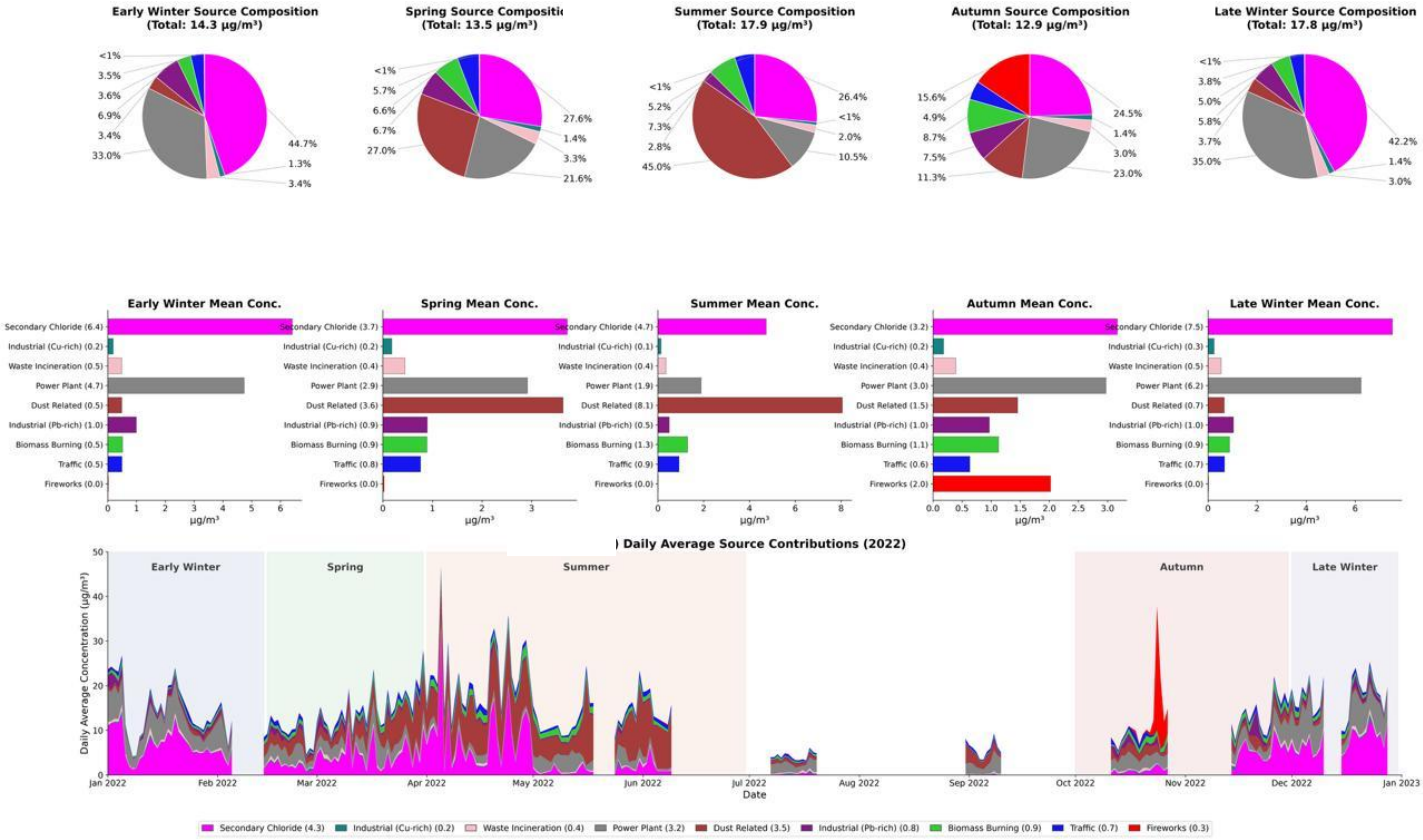

HOA
BBOA (Fresh)
BBOA(Aged)
MO-OOA
LO-OOA
μg m⁻³
time (hour)
Season
Early Winter
Spring
Summer
Autumn
Late Winter



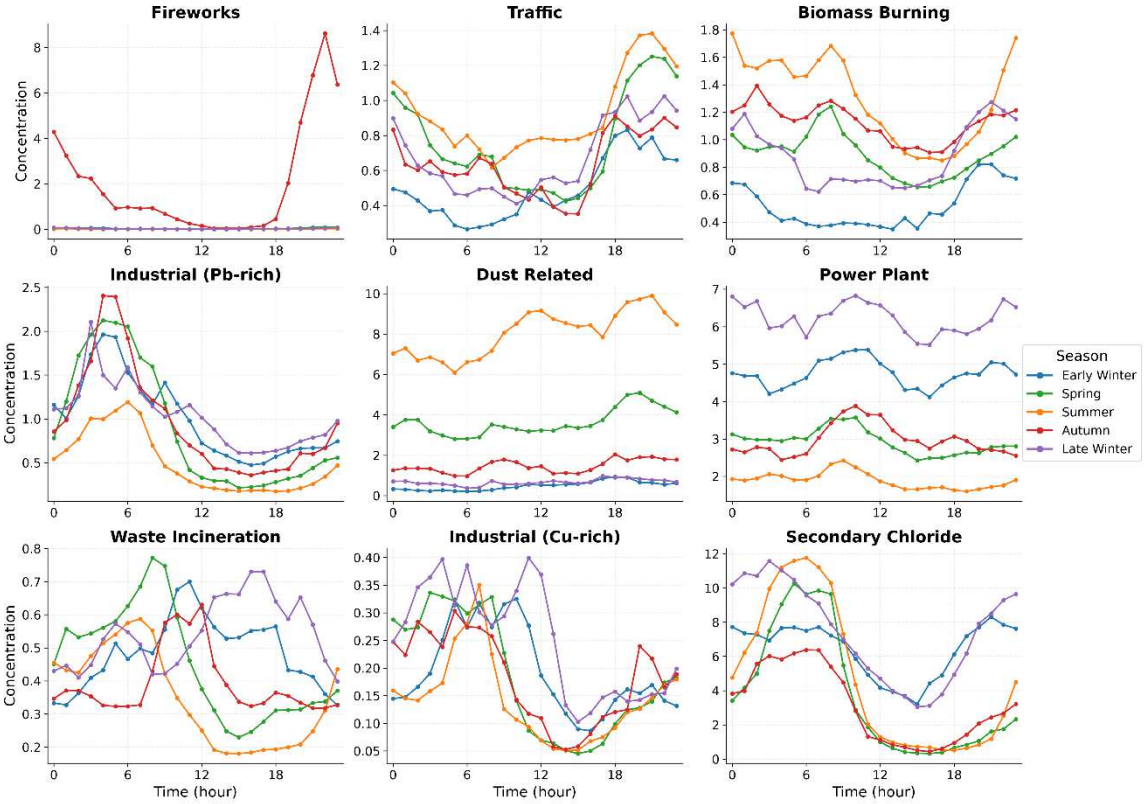
c

Figure 2. Seasonal source apportionment of organic aerosols (OA). (a) Top present pie charts of OA factors resolved by PMF and bar plots of seasonal mean concentrations, including hydrocarbon-like OA (HOA), fresh and aged biomass burning OA (BBOA), semi-volatile OOA (SVOOA), and low-volatility OOA (LVOOA). Bottom Panels show daily OA factor concentrations across seasons, with highest contributions in early winter and autumn. (b) Diurnal profiles reveal strong rush-hour peaks for HOA, pronounced morning and nighttime peaks for fresh BBOA, and enhanced aged BBOA and OOA during stable nighttime periods. LVOOA and SVOOA showed persistent daytime contributions, consistent with secondary formation processes (c)

a


Early Winter Source Composition
(Total: 14.3 µg/m³)
<1%
3.5%
3.6%
6.9%
3.4%
33.0%
44.7%
1.3%
3.4%
Spring Source Composition
(Total: 13.5 µg/m³)
<1%
5.7%
6.6%
6.7%
27.0%
27.6%
1.4%
3.3%
21.6%
Summer Source Composition
(Total: 17.9 µg/m³)
<1%
5.2%
7.3%
2.8%
45.0%
26.4%
<1%
2.0%
10.5%
Autumn Source Composition
(Total: 12.9 µg/m³)
15.6%
4.9%
8.7%
7.5%
11.3%
24.5%
1.4%
3.0%
23.0%
Late Winter Source Composition
(Total: 17.8 µg/m³)
<1%
3.8%
5.0%
5.8%
3.7%
35.0%
42.2%
1.4%
3.0%
Early Winter Mean Conc.
Secondary Chloride (6.4)
Industrial (Cu-rich) (0.2)
Waste Incineration (0.5)
Power Plant (4.7)
Dust Related (0.5)
Industrial (Pb-rich) (1.0)
Biomass Burning (0.5)
Traffic (0.5)
Fireworks (0.0)
µg/m³
Spring Mean Conc.
Secondary Chloride (3.7)
Industrial (Cu-rich) (0.2)
Waste Incineration (0.4)
Power Plant (2.9)
Dust Related (3.6)
Industrial (Pb-rich) (0.9)
Biomass Burning (0.9)
Traffic (0.8)
Fireworks (0.0)
µg/m³
Summer Mean Conc.
Secondary Chloride (4.7)
Industrial (Cu-rich) (0.1)
Waste Incineration (0.4)
Power Plant (1.9)
Dust Related (8.1)
Industrial (Pb-rich) (0.5)
Biomass Burning (1.3)
Traffic (0.9)
Fireworks (0.0)
µg/m³
Autumn Mean Conc.
Secondary Chloride (3.2)
Industrial (Cu-rich) (0.2)
Waste Incineration (0.4)
Power Plant (3.0)
Dust Related (1.5)
Industrial (Pb-rich) (1.0)
Biomass Burning (1.1)
Traffic (0.6)
Fireworks (2.0)
µg/m³
Late Winter Mean Conc.
Secondary Chloride (7.5)
Industrial (Cu-rich) (0.3)
Waste Incineration (0.5)
Power Plant (6.2)
Dust Related (0.7)
Industrial (Pb-rich) (1.0)
Biomass Burning (0.9)
Traffic (0.7)
Fireworks (0.0)
µg/m³
Daily Average Source Contributions (2022)
Early Winter
Spring
Summer
Autumn
Late Winter
Daily Average Concentration (µg/m³)
Jan 2022
Feb 2022
Mar 2022
Apr 2022
May 2022
Jun 2022
Jul 2022
Aug 2022
Sep 2022
Oct 2022
Nov 2022
Dec 2022
Jan 2023
Date
Secondary Chloride (4.3)
Industrial (Cu-rich) (0.2)
Waste Incineration (0.4)
Power Plant (3.2)
Dust Related (3.5)
Industrial (Pb-rich) (0.8)
Biomass Burning (0.9)
Traffic (0.7)
Fireworks (0.3)

b


Fireworks
Traffic
Biomass Burning
Industrial (Pb-rich)
Dust Related
Power Plant
Waste Incineration
Industrial (Cu-rich)
Secondary Chloride
Concentration
Time (hour)
Season
Early Winter
Spring
Summer
Autumn
Late Winter

c

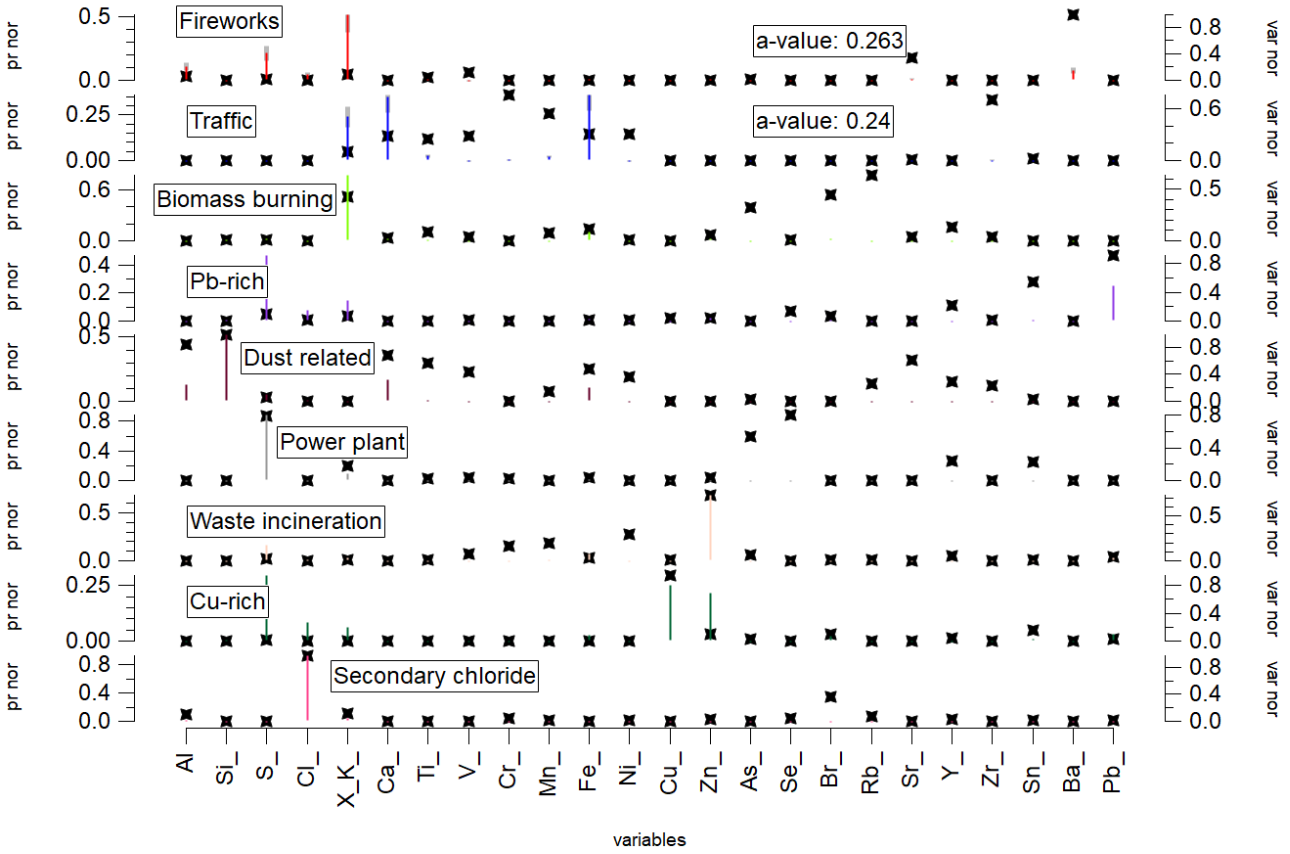


Figure 3. Source apportionment of elemental $PM_{2.5}$ and diurnal variability of sources. (a) Top Panels display seasonal source compositions and mean concentrations derived from PMF, showing contributions from Secondary Chloride, Dust Related, Power Plant, Biomass Burning, Industrial (Pb-rich and Cu-rich), Waste Incineration, Traffic, and Fireworks. Bottom Panel presents daily average source contributions, highlighting dust peaks in summer, post-monsoon fireworks episodes, and elevated Secondary Chloride and Power Plant contributions in winter. Lower panels show diurnal patterns of individual sources. (b) Traffic and Biomass Burning exhibit distinct morning and evening peaks, Dust Related shows both daytime and nighttime enhancements linked to resuspension, and Secondary Chloride displays strong daytime minima due to volatility. Power Plant shows weak diurnality, consistent with continuous emissions, while industrial and waste incineration sources exhibit nighttime enhancements. Seasonal differences emphasize the combined influence of meteorology, boundary layer dynamics, and source activity patterns (c) Factor profile of resolved elemental factor

Supplementary Files

This is a list of supplementary files associated with this preprint. Click to download.

- supplementarydelhi.docx